Rotational structures in ^{177}Ta

D. E. Archer, M. A. Riley, T. B. Brown, J. Döring, D. J. Hartley, G. D. Johns, T. D. Johnson,* R. A. Kaye, J. Pfohl, and S. L. Tabor
Department of Physics, Florida State University, Tallahassee, Florida 32306

J. Simpson
C.C.L. Daresbury Laboratory, Warrington, WA4 4AD, United Kingdom

Yang Sun
Joint Institute of Heavy Ion Research, Oak Ridge, Tennessee 37831
and Department of Physics and Atmospheric Science, Drexel University, Philadelphia, Pennsylvania 19104
(Received 9 May 1995)

High-spin states in ^{177}Ta were produced using the ^{170}Er(^{11}B, $4n$) reaction at 55 and 60 MeV. Considerable extensions have been made to the previously known level scheme, and new structures have been found. $B(M1)/B(E2)$ ratios have been extracted for strongly coupled bands. The behavior of the different rotational cascades, in particular the anomalous crossing frequency observed in the $[541]\frac{1}{2}^-$ proton $h_{9/2}$ band and the occurrence of "identical bands," is discussed. Comparisons are made with projected shell model calculations.

PACS number(s): 21.10.Re, 21.60.Cs, 23.20.Lv, 27.70.+q

I. INTRODUCTION

The $N=104$ odd-Z nucleus ^{177}Ta lies in the upper part of the deformed rare-earth region where the quadrupole ground-state deformation of neighboring even-even nuclei is reasonably stable with respect to the neutron number. In odd-Z nuclei, the strong polarizing influence of particular proton orbitals can, however, produce substantial changes to the deformation, alignments, and moments of inertia of rotational sequences built on single-quasiproton states. Indeed several odd-Z nuclei around $A = 175$ (^{177}Ta included) were singled out for special discussion with regard to the remarkable phenomenon of "identical" bands in normal deformed nuclei [1,2]. The finding that certain single (and even higher seniority) quasiparticle (qp) excitations have identical moments of inertia to those of the neighboring ground-state even-even band was at odds with our conventional understanding of the blocking effect [3]. An attempt to explain the effect on the moment of inertia in terms of specific cancellations of pairing, mass, alignment, and deformation has been put forward [1,2]. Some initial results from the present study which tended to support this particular explanation of identical bands in ^{177}Ta have already been published [4].

In an odd-Z even-N rare earth nucleus, the first $i_{13/2}$ neutron alignment or backbend is expected to occur at about the same rotational frequency ($\hbar\omega_c \sim 0.3$ MeV) in each rotational sequence. This simple expectation seems to hold true experimentally except for bands based on the $h_{9/2}[541]\frac{1}{2}^-$ orbital. In the latter case, the backbending has been found systematically to be delayed in rotational frequency compared to the other bands; see for example Ref. [5]. The interpretation of this anomalous backbending behavior of the proton $h_{9/2}[541]\frac{1}{2}^-$ rotational band has been a long-standing problem. Configuration-dependent shape effects, in which the occupation of this deformation driving orbit polarizes the nucleus to larger β_2 values, form an important ingredient in any explanation of this problem but they are not able to satisfactorily explain the full extent of the delayed band crossing frequencies observed. Recently, Sun, Wen, and Feng [6] proposed an answer to this problem using angular momentum projection theory which included the quadrupole pairing interaction. These calculations seemed to explain in a consistent manner the delayed backbending observed in $h_{9/2}$ bands in a long chain of Ta isotopes ranging from $A = 167$ to 175. It is therefore of interest to see if this theoretical framework correctly predicts the behavior of this band in ^{177}Ta. Another recent study of this band crossing anomally has also been performed by Wu [7] using the particle-rotor framework.

The large signature splitting of the $[541]\frac{1}{2}^-$ orbital means that the unfavored branch has rarely been observed experimentally due to its high excitation energy above the yrast line. Therefore it has not been possible to determine if the same anomalous backbending behavior is also present in the unfavored sequence. In the present experiment it has been possible to extend the unfavored $[541]\frac{1}{2}^-$ band in ^{177}Ta to spin values in the backbending region and address this question.

Another interesting aspect of nuclei in this region is the presence of high-K isomers. A comprehensive study of isomers in ^{177}Ta has recently been published by Dasgupta *et al.* [8] and will therefore not be discussed in the present work. In addition, Dasgupta *et al.* [9] have also reported briefly on some of the prompt rotational cascades in ^{177}Ta in agreement with our present measurements.

II. EXPERIMENTAL METHODS AND RESULTS

High-spin states in ^{177}Ta were produced using the ^{170}Er(^{11}B, $4n$) reaction at two different beam energies. The

*Present address: Department of Physics, University of Notre Dame, Notre Dame, IN 46556.

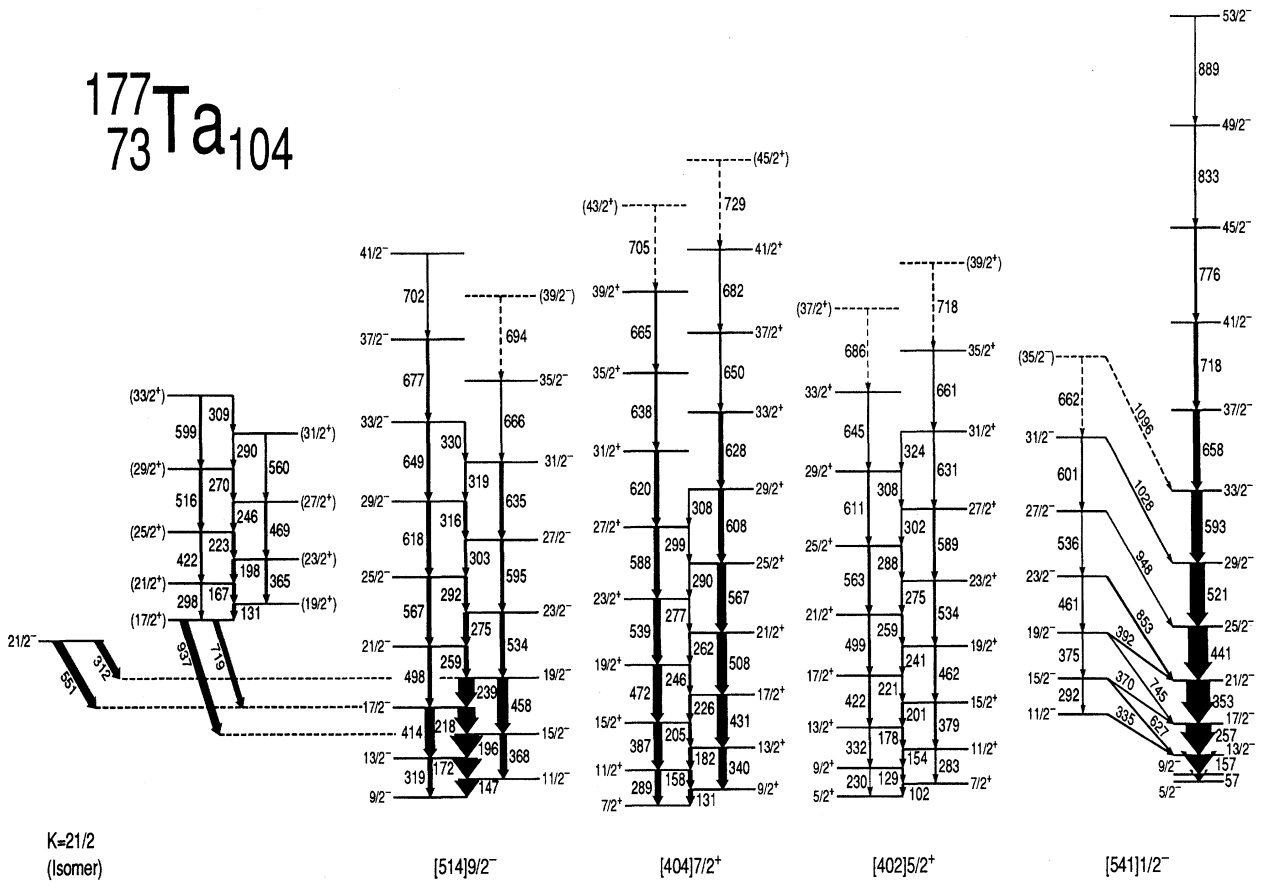

FIG. 1. Level scheme for prompt rotational bands in ^{177}Ta. A comprehensive level scheme for isomeric structures may be found in Ref. [8].

beam was provided by the FN Tandem and the Superconducting Linear Accelerator at Florida State University. The first experiment used a beam energy of 55 MeV on two self-supporting 1 mg/cm^2 foils of ^{170}Er. The deexcitation γ rays were detected in an array of five escape suppressed spectrometers [10]. A total of 5×10^7 coincidence events were collected when two or more suppressed Ge detectors were in prompt ($\leq$ 100 ns) coincidence. Some of the results from this experiment have been reported previously [4].

A second experiment was run with the same reaction but with a beam energy of 60 MeV in order to enhance the population of the higher spin-states. This experiment employed two self-supporting 1 mg/cm^2 foils of ^{170}Er, and the Pittsburgh–Florida State γ array [11] consisting of 10 escape suppressed Ge detectors [10] plus a 28-element BGO multiplicity filter. A total of 8×10^7 prompt γ-γ events was collected when two or more suppressed Ge detectors were in prompt coincidence.

The spectra from the Ge detectors were gain matched off line, and a $4k\times4k$ matrix was created for each experiment separately using all possible combinations of coincidence pairs. The γ-ray energy and detection efficiency were calibrated using ^{152}Eu and ^{133}Ba sources. The low-energy portion of the efficiency curve of the experiment at 60 MeV was supplemented by γ-γ coincidence efficiency information taken using this setup on a nearby well-deformed even-even nucleus. The γ-ray coincidence data were mainly analyzed using the program ESCL8R created by Radford [12].

A. Level scheme of ^{177}Ta

Prior work on this nucleus had identified four rotational bands based upon different quasiproton excitations, $[541]\frac{1}{2}^-$, $[514]\frac{9}{2}^-$, $[404]\frac{7}{2}^+$, and $[402]\frac{5}{2}^+$, up to spins $I^\pi = \frac{29}{2}^-$, $\frac{23}{2}^-$, $\frac{17}{2}^+$, and $\frac{19}{2}^+$, respectively [13–15]. In the present study, these rotational bands have been extended to $I^\pi = \frac{53}{2}^-$, $\frac{41}{2}^-$, $(\frac{45}{2}^+)$, and $(\frac{39}{2}^+)$, respectively. In addition, the unfavored signature of the $[541]\frac{1}{2}^-$ band has been tentatively observed to a spin of $\frac{35}{2}^-$, based on earlier work by Schilling *et al.* [15] who observed states in this band up to $\frac{19}{2}^-$. Also, a new strongly coupled sequence has been found.

The level scheme for ^{177}Ta obtained from the present study is shown in Fig. 1 and includes over 90 new γ rays. Table I lists excitation energies, transition energies, relative γ ray intensities, branching ratios, and spin and parity assignments.

1. Band based upon the proton $[541]\frac{1}{2}^-$ *Nilsson state*

This is the most intensely populated band in ^{177}Ta. Figure 2(a) shows a spectrum for this rotational band, with the inset especially selected to highlight the uppermost transitions

TABLE I. Data for ^{177}Ta.

E_x(keV) [a]	E_γ(keV) [b]	I_γ^{rel} [c]	λ [d]	I_i^π	I_f^π [e]
$[541]\frac{1}{2}^-$, $\alpha = +\frac{1}{2}$					
243.1	57.0			$\frac{9}{2}^-$	$\frac{5}{2}^-$
399.9	156.8			$\frac{13}{2}^-$	$\frac{9}{2}^-$
656.8	256.9	100		$\frac{17}{2}^-$	$\frac{13}{2}^-$
1009.4	352.6	94±2		$\frac{21}{2}^-$	$\frac{17}{2}^-$
1450.5	441.1	79±2		$\frac{25}{2}^-$	$\frac{21}{2}^-$
1971.7	521.2	59±1		$\frac{29}{2}^-$	$\frac{25}{2}^-$
2564.7	593.0	44±1		$\frac{33}{2}^-$	$\frac{29}{2}^-$
3222.6	657.9	27±1		$\frac{37}{2}^-$	$\frac{33}{2}^-$
3940.2	717.6	15±1		$\frac{41}{2}^-$	$\frac{37}{2}^-$
4715.7	775.5	9.0±0.5		$\frac{45}{2}^-$	$\frac{41}{2}^-$
5548.4	832.7	6.0±0.5		$\frac{49}{2}^-$	$\frac{45}{2}^-$
6437.3	888.9	3.0±0.5		$\frac{53}{2}^-$	$\frac{49}{2}^-$
$[541]\frac{1}{2}^-$, $\alpha=-\frac{1}{2}$					
734.5	334.7	1.0±0.5		$\frac{11}{2}^-$	$\frac{13}{2}^-$
1027.0	292.0	2.0±0.5		$\frac{15}{2}^-$	$\frac{11}{2}^-$
	370.2	3.0±0.5	0.76±0.18	$\frac{15}{2}^-$	$\frac{17}{2}^-$
	627.1	1.0±0.5	1.9±1.5	$\frac{15}{2}^-$	$\frac{13}{2}^-$
1401.7	374.5	3.0±0.5		$\frac{19}{2}^-$	$\frac{15}{2}^-$
	392.0	2.0±0.5	1.08±0.22	$\frac{19}{2}^-$	$\frac{21}{2}^-$
	745.2	3±1	0.83±0.19	$\frac{19}{2}^-$	$\frac{17}{2}^-$
1862.5	460.8	6.0±0.5	1.06±0.15	$\frac{23}{2}^-$	$\frac{19}{2}^-$
	853.1	6±1		$\frac{23}{2}^-$	$\frac{21}{2}^-$
2398.1	535.6	4.0±0.5	1.21±0.21	$\frac{27}{2}^-$	$\frac{23}{2}^-$
	947.6	3.0±0.5		$\frac{27}{2}^-$	$\frac{25}{2}^-$
2999.2	601.1	8±1	3.8±0.8	$\frac{31}{2}^-$	$\frac{27}{2}^-$
	1028.1	2.0±0.5		$\frac{31}{2}^-$	$\frac{29}{2}^-$
3661.2	662.2	1.0±0.5	0.76±0.31	$(\frac{35}{2}^-)$	$\frac{31}{2}^-$
	1096.4	2.0±0.5		$(\frac{35}{2}^-)$	$\frac{33}{2}^-$
$[514]\frac{9}{2}^-$, $\alpha = +\frac{1}{2}$					
392.3	318.8	17±4	0.20±0.04	$\frac{13}{2}^-$	$\frac{9}{2}^-$
	171.9	87±3		$\frac{13}{2}^-$	$\frac{11}{2}^-$
806.4	414.1	39±1	0.56±0.02	$\frac{17}{2}^-$	$\frac{13}{2}^-$
	218.4	71±2		$\frac{17}{2}^-$	$\frac{15}{2}^-$
1304.3	497.9	16±1	0.88±0.05	$\frac{21}{2}^-$	$\frac{17}{2}^-$
	258.8	19±1		$\frac{21}{2}^-$	$\frac{19}{2}^-$
1871.4	567.2	17±1	1.22±0.07	$\frac{25}{2}^-$	$\frac{21}{2}^-$
	292.3	14±1		$\frac{25}{2}^-$	$\frac{23}{2}^-$
2489.8	618.2	18±1	1.41±0.08	$\frac{29}{2}^-$	$\frac{25}{2}^-$
	316.0	13±1		$\frac{29}{2}^-$	$\frac{27}{2}^-$
3138.5	648.7	15±1	1.85±0.13	$\frac{33}{2}^-$	$\frac{29}{2}^-$
	329.5	8±1		$\frac{33}{2}^-$	$\frac{31}{2}^-$
3815.5	677.0	10±1		$\frac{37}{2}^-$	$\frac{33}{2}^-$
4517.3	701.8	5±1		$\frac{41}{2}^-$	$\frac{37}{2}^-$
$[514]\frac{9}{2}^-$, $\alpha=-\frac{1}{2}$					
220.4	146.9			$\frac{11}{2}^-$	$\frac{9}{2}^-$
588.0	367.6	29±1	0.31±0.01	$\frac{15}{2}^-$	$\frac{11}{2}^-$
	195.7	95±2		$\frac{15}{2}^-$	$\frac{13}{2}^-$
1045.4	457.5	46±1	0.73±0.02	$\frac{19}{2}^-$	$\frac{15}{2}^-$
	239.0	64±1		$\frac{19}{2}^-$	$\frac{17}{2}^-$
1579.3	534.0	19±1	0.87±0.05	$\frac{23}{2}^-$	$\frac{19}{2}^-$
	275.0	22±1		$\frac{23}{2}^-$	$\frac{21}{2}^-$
2173.9	594.6	14±1	1.23±0.08	$\frac{27}{2}^-$	$\frac{23}{2}^-$
	302.6	12±1		$\frac{27}{2}^-$	$\frac{25}{2}^-$

TABLE I. (*Continued*).

E_x(keV) [a]	E_γ(keV) [b]	I_γ^{rel} [c]	λ [d]	I_i^π	I_f^π [e]
2809.0	636.2	16±1	1.90±0.14	$\frac{31}{2}^-$	$\frac{27}{2}^-$
	318.8	8±1		$\frac{31}{2}^-$	$\frac{29}{2}^-$
3475.1	666.1	5±1		$\frac{35}{2}^-$	$\frac{31}{2}^-$
4168.7	693.6	5±1		$(\frac{39}{2}^-)$	$\frac{35}{2}^-$
$[404]\frac{7}{2}^+$, $\alpha = -\frac{1}{2}$					
288.8	288.8	25±3	1.42±0.16	$\frac{11}{2}^+$	$\frac{7}{2}^+$
	157.5	18±2		$\frac{11}{2}^+$	$\frac{9}{2}^+$
676.1	387.3	34±2	2.88±0.17	$\frac{15}{2}^+$	$\frac{11}{2}^+$
	205.1	12±1		$\frac{15}{2}^+$	$\frac{13}{2}^+$
1147.8	471.7	36±1	4.37±0.28	$\frac{19}{2}^+$	$\frac{15}{2}^+$
	245.7	8.0±0.5		$\frac{19}{2}^+$	$\frac{17}{2}^+$
1687.2	539.3	28±1	4.66±0.35	$\frac{23}{2}^+$	$\frac{19}{2}^+$
	277.4	6.0±0.5		$\frac{23}{2}^+$	$\frac{21}{2}^+$
2275.7	588.4	23±1	3.87±0.26	$\frac{27}{2}^+$	$\frac{23}{2}^+$
	299.3	6.0±0.5		$\frac{27}{2}^+$	$\frac{25}{2}^+$
2895.9	620.2	20±1		$\frac{31}{2}^+$	$\frac{27}{2}^+$
3533.9	638.0	12±1		$\frac{35}{2}^+$	$\frac{31}{2}^+$
4198.4	664.5	9.0±0.5		$\frac{39}{2}^+$	$\frac{35}{2}^+$
4903.4	705.0	4.0±0.5		$(\frac{43}{2}^+)$	$\frac{39}{2}^+$
$[404]\frac{7}{2}^+$, $\alpha = +\frac{1}{2}$					
131.3	131.3			$\frac{9}{2}^+$	$\frac{7}{2}^+$
471.0	339.7	32±2	2.03±0.12	$\frac{13}{2}^+$	$\frac{9}{2}^+$
	182.1	16±1		$\frac{13}{2}^+$	$\frac{11}{2}^+$
902.4	431.4	43±4	3.61±0.17	$\frac{17}{2}^+$	$\frac{13}{2}^+$
	226.3	12±1		$\frac{17}{2}^+$	$\frac{15}{2}^+$
1410.2	507.8	39±1	5.03±0.30	$\frac{21}{2}^+$	$\frac{17}{2}^+$
	262.1	8.0±0.5		$\frac{21}{2}^+$	$\frac{19}{2}^+$
1976.7	566.5	35±1	5.95±0.41	$\frac{25}{2}^+$	$\frac{21}{2}^+$
	289.6	6.0±0.5		$\frac{25}{2}^+$	$\frac{23}{2}^+$
2584.0	607.5	21±1	5.9±0.7	$\frac{29}{2}^+$	$\frac{25}{2}^+$
	307.5	4.0±0.5		$\frac{29}{2}^+$	$\frac{27}{2}^+$
3212.1	628.1	17±1		$\frac{33}{2}^+$	$\frac{29}{2}^+$
3862.3	650.2	6±1		$\frac{37}{2}^+$	$\frac{33}{2}^+$
4544.0	681.7	5±1		$\frac{41}{2}^+$	$\frac{37}{2}^+$
5273.0	729.0	3.0±0.5		$(\frac{45}{2}^+)$	$\frac{41}{2}^+$
$[402]\frac{5}{2}^+$, $\alpha = +\frac{1}{2}$					
300.2	229.6	3±1	0.37±0.15	$\frac{9}{2}^+$	$\frac{5}{2}^+$
	128.8[f]	8±1		$\frac{9}{2}^+$	$\frac{7}{2}^+$
632.1	331.9	6.0±0.5	0.66±0.06	$\frac{13}{2}^+$	$\frac{9}{2}^+$
	178.1	9±1		$\frac{13}{2}^+$	$\frac{11}{2}^+$
1054.4	422.2	8.0±0.5	1.00±0.08	$\frac{17}{2}^+$	$\frac{13}{2}^+$
	221.3	8.0±0.5		$\frac{17}{2}^+$	$\frac{15}{2}^+$
1553.6	499.1	10±1	1.15±0.10	$\frac{21}{2}^+$	$\frac{17}{2}^+$
	258.7	9.0±0.5		$\frac{21}{2}^+$	$\frac{19}{2}^+$
2116.8	563.3	11±1	1.62±0.13	$\frac{25}{2}^+$	$\frac{21}{2}^+$
	288.2	7±1		$\frac{25}{2}^+$	$\frac{23}{2}^+$
2727.7	611.1	8±1	2.27±0.26	$\frac{29}{2}^+$	$\frac{25}{2}^+$
	307.9[f]	4.0±0.5		$\frac{29}{2}^+$	$\frac{27}{2}^+$
3372.7	645.0	5.0±0.5		$\frac{33}{2}^+$	$\frac{29}{2}^+$
4058.7	686.0	3.0±0.5		$(\frac{37}{2}^+)$	$\frac{33}{2}^+$
$[402]\frac{5}{2}^+$, $\alpha = -\frac{1}{2}$					
172.0	101.9			$\frac{7}{2}^+$	$\frac{5}{2}^+$
454.4	282.9	5±1	0.42±0.10	$\frac{11}{2}^+$	$\frac{7}{2}^+$
	153.8	12±1		$\frac{11}{2}^+$	$\frac{9}{2}^+$
833.2	378.8	8±1	0.74±0.06	$\frac{15}{2}^+$	$\frac{11}{2}^+$

TABLE I. (*Continued*).

E_x(keV) [a]	E_γ(keV) [b]	I_γ^{rel} [c]	λ [d]	I_i^π	I_f^π [e]
	201.0	11±1		$\frac{15}{2}^+$	$\frac{13}{2}^+$
1295.0	462.0	10±1	1.31±0.11	$\frac{19}{2}^+$	$\frac{15}{2}^+$
	240.5	7.0±0.5		$\frac{19}{2}^+$	$\frac{17}{2}^+$
1828.5	533.6	9.0±0.5	1.39±0.12	$\frac{23}{2}^+$	$\frac{19}{2}^+$
	274.7	7.0±0.5		$\frac{23}{2}^+$	$\frac{21}{2}^+$
2419.0	588.9[f]	9±1	1.83±0.18	$\frac{27}{2}^+$	$\frac{23}{2}^+$
	301.6	5.0±0.5		$\frac{27}{2}^+$	$\frac{25}{2}^+$
3050.1	630.6	7.0±0.5	2.27±0.31	$\frac{31}{2}^+$	$\frac{27}{2}^+$
	324.1[f]	3.0±0.5		$\frac{31}{2}^+$	$\frac{29}{2}^+$
3711.2	661.1	6.0±0.5		$\frac{35}{2}^+$	$\frac{31}{2}^+$
4429.5	718.3	2.0±0.5		$(\frac{39}{2}^+)$	$\frac{35}{2}^+$
$\pi[514]\frac{9}{2}^- \otimes \nu([633]\frac{7}{2}^+,[521]\frac{1}{2}^-)$, $\alpha = -\frac{1}{2}$					
1525.0	937.0	20±2	2.25±0.17	$(\frac{17}{2}^+)$	$\frac{15}{2}^-$
	718.8	13±1		$(\frac{17}{2}^+)$	$\frac{17}{2}^-$
1823.2	298.0	4.0±0.5	0.27±0.03	$(\frac{21}{2}^+)$	$(\frac{17}{2}^+)$
	167.1	14.0±0.5		$(\frac{21}{2}^+)$	$(\frac{19}{2}^+)$
2244.4	421.7	8.0±0.5	0.6±0.4	$(\frac{25}{2}^+)$	$(\frac{21}{2}^+)$
	223.0	13.0±0.5		$(\frac{25}{2}^+)$	$(\frac{23}{2}^+)$
2760.1	515.7	11.0±0.5	1.23±0.08	$(\frac{29}{2}^+)$	$(\frac{25}{2}^+)$
	269.9	9.0±0.5		$(\frac{29}{2}^+)$	$(\frac{27}{2}^+)$
3358.9	598.7	10±1	1.6±0.1	$(\frac{33}{2}^+)$	$(\frac{29}{2}^+)$
	308.8	6±1		$(\frac{33}{2}^+)$	$(\frac{31}{2}^+)$
$\pi[514]\frac{9}{2}^- \otimes \nu([633]\frac{7}{2}^+,[521]\frac{1}{2}^-)$, $\alpha = +\frac{1}{2}$					
1656.2	131.2	10.0±0.5	0.54±0.07	$(\frac{19}{2}^+)$	$(\frac{17}{2}^+)$
2020.9	364.8	10.0±0.5	0.65±0.04	$(\frac{23}{2}^+)$	$(\frac{19}{2}^+)$
	197.5	16.0±0.5		$(\frac{23}{2}^+)$	$(\frac{21}{2}^+)$
2490.2	469.1	10.0±0.5	1.06±0.07	$(\frac{27}{2}^+)$	$(\frac{23}{2}^+)$
	246.0	9.0±0.5		$(\frac{27}{2}^+)$	$(\frac{25}{2}^+)$
3050.2	560.0	6.0±0.5	1.10±0.11	$(\frac{31}{2}^+)$	$(\frac{27}{2}^+)$
	290.0	6.0±0.5		$(\frac{31}{2}^+)$	$(\frac{29}{2}^+)$

[a]Level energies; bandhead excitation energies have been taken from previous work [13–15].
[b]Accurate to 0.2 keV for most transitions. For weak or contaminated transitions, accurate to 0.5 keV.
[c]Relative γ-ray intensities [$I_\gamma(256.9)\equiv 100$] measured predominantly from the 156.8 keV gated spectrum from the 60 MeV data set. For γ-ray doublets other pertinent coincidence spectra were used.
[d]Branching ratio $\lambda = I_\gamma(I\rightarrow I-2)/I_\gamma(I\rightarrow I-1)$ measured from spectra corresponding to gates above spin I.
[e]Spin and parity assignments are based on the previous work [13–15] and on the assumption that the character of the new transitions within bands continues being stretched $E2$ in nature.
[f]Accurate to within 1 keV.

within the band. Prior to our work this band had been observed up to the 521 keV $\frac{29}{2}^- \rightarrow \frac{25}{2}^-$ transition. Results for this band from the present work were first reported in Ref. [4]; however, our second experiment performed at 60 MeV has convinced us that the $\frac{53}{2}^- \rightarrow \frac{49}{2}^-$ transition is of energy 889 keV and not 896 keV; see the inset of Fig. 2(a). The unfavored $\alpha = -\frac{1}{2}$ signature partner has been observed. Previously, transitions from the $\frac{19}{2}^-$, $\frac{15}{2}^-$, and $\frac{11}{2}^-$ levels to the favored $[541]\frac{1}{2}^-$ sequence had been observed [15]. This study confirms these decays and extends the $\alpha = -\frac{1}{2}$ signature band to a tentative spin of $\frac{35}{2}^-$.

2. *Band based upon the proton* $[514]\frac{9}{2}^-$ *Nilsson state*

Figure 2(b) shows a spectrum for this rotational band gated on the 316 keV intraband transition. Previously this band had been observed up to the 534 keV $\frac{23}{2}^- \rightarrow \frac{19}{2}^-$ transition. This band is strongly fed by the $\frac{21}{2}^-$ isomeric state at excitation energy $E_x = 1.357$ MeV by transitions of 312 and 551 keV into the $\frac{19}{2}^-$ and $\frac{17}{2}^-$ levels, respectively, as indicated in Fig. 1. The multiquasiparticle configurations built upon the $\frac{21}{2}^-$ isomeric state have been discussed by Dasgupta *et al.* [8]. The $[514]\frac{9}{2}^-$ sequence continues above these feeding points and is observed up to spin $\frac{41}{2}^-$.

3. *Band based upon the proton* $[404]\frac{7}{2}^+$ *Nilsson state*

A spectrum for this band can be seen in Fig. 2(c) with the inserts highlighting the upper high-spin transitions in the two signature sequences now observed tentatively up to spins $\frac{45}{2}^+$ and $\frac{43}{2}^+$. Previously this band had been observed up to the 431 keV $\frac{17}{2}^+ \rightarrow \frac{13}{2}^+$ transition.

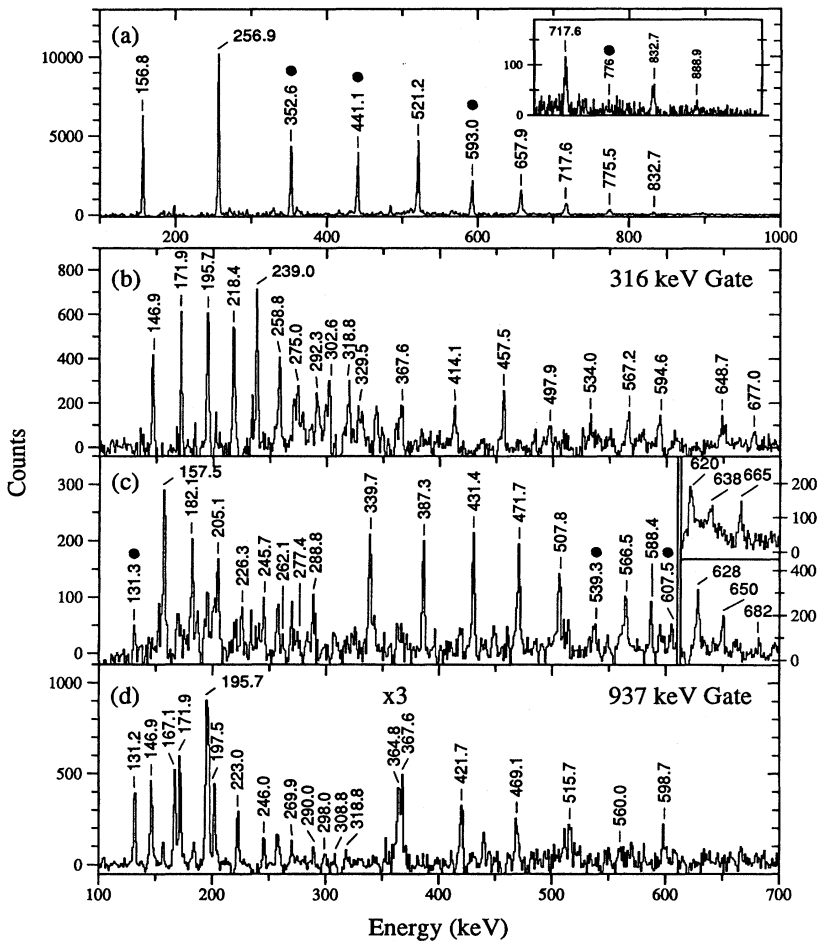

FIG. 2. Coincidence γ-ray spectra for the (a) $[541]\frac{1}{2}^-$, (b) $[514]\frac{9}{2}^-$, (c) $[404]\frac{7}{2}^+$, and (d) the new strongly coupled bands in ^{177}Ta. The inset in panel (a) is a mathematical AND [12] between the 776 keV gate and the sum of the 658 and 718 keV gates highlighting the low-intensity high-spin states of the $[541]\frac{1}{2}^-$ band. Panel (c) was taken by a mathematical AND between the 131 keV gate and the sum of the 539 and 608 keV gates. The upper inset of panel (c) highlights the high spins of the $\alpha=-\frac{1}{2}$ band with a mathematical AND between the 472 and 588 keV gates, and the lower inset highlights the $\alpha=+\frac{1}{2}$ band with an AND between the 508 and 608 keV gates. Panel (d) has been multiplied by a factor of 3 above 350 keV.

4. Band based upon the proton $[402]\frac{5}{2}^+$ *Nilsson state*

Previously this band had been observed up to the 462 keV $\frac{19}{2}^+ \rightarrow \frac{15}{2}^+$ transition. A spectrum of this weakly populated band has been previously published from our work [4] where an extension up to a tentative spin of $\frac{39}{2}^+$ was established.

5. New strongly coupled sequence

Figure 2(d) shows a gate on the 937 keV γ ray connecting a new strongly coupled structure to the $[514]\frac{9}{2}^-$ band. This new structure decays into the $[514]\frac{9}{2}^-$ band at the $\frac{15}{2}^-$ and $\frac{17}{2}^-$ levels; see Fig. 1. Spin and parity assignments to this structure are based on the observed intensity in relation to its excitation energy, its likely configuration (see later), and the fact that the 937 keV decay has an angular correlation measurement consistent with it being of stretched dipole character. In addition, the 719 decay has an angular correlation ratio consistent with that expected for an unstretched dipole transition.

III. ELECTROMAGNETIC PROPERTIES: $B(M1)/B(E2)$ VALUES

The experimental $B(M1)/B(E2)$ ratios have been calculated using the observed γ-ray energies and branching ratios (λ) according to the standard formula

$$\frac{B(M1:I\rightarrow I-1)}{B(E2:I\rightarrow I-2)}=0.693\frac{E_\gamma^5(I\rightarrow I-2)}{E_\gamma^3(I\rightarrow I-1)}\times\frac{1}{\lambda(1+\delta^2)}\left(\frac{\mu_N}{e\ \mathrm{b}}\right)^2,$$

where E_γ is in MeV. In our calculations, as is commonplace in such simple analyses without introducing unreasonably large uncertainties, a mixing ratio (δ) of zero has been assumed.

The experimental $B(M1)/B(E2)$ values as a function of spin for the $[514]\frac{9}{2}^-$, $[404]\frac{7}{2}^+$, and $[402]\frac{5}{2}^+$ bands can be seen in Fig. 3(a). A similar plot for the new strongly coupled band is shown in Fig. 3(b).

Theoretical calculations have been made using 1qp and 3qp configurations. For the $B(M1)$ calculation an extended formalism [16] of the geometrical model proposed by Dönau [17] has been used:

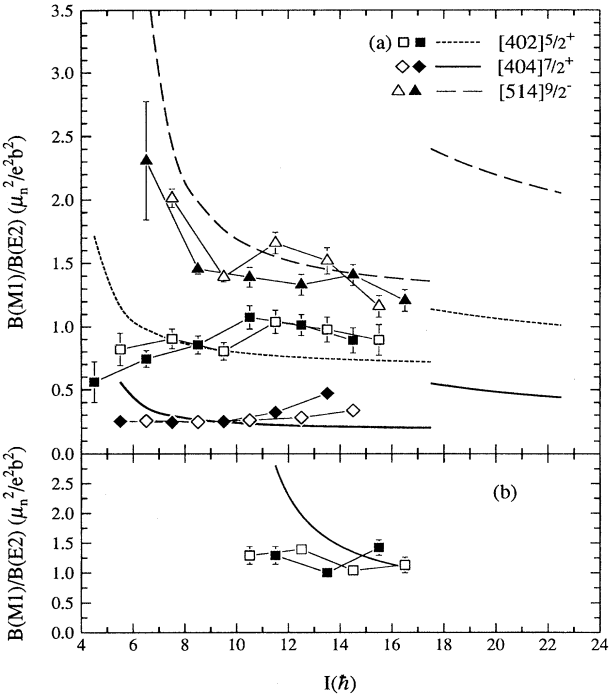

FIG. 3. Experimental $B(M1)/B(E2)$ ratios as a function of spin for bands in ^{177}Ta. The theoretical predictions of the geometrical model of Dönau are also shown. Panel (a) contains the main rotational structures and panel (b) shows the new strongly coupled band. Curves above $I=17\hbar$ in panel (a) indicate the expectations for the aligned bands after the $i_{13/2}$ neutron band crossing.

$$B(M1;I\rightarrow I-1)$$
$$=\frac{3}{8\pi I^2}\left\{\sqrt{I^2-K^2}\left[\left(1\pm\frac{\Delta e'}{\hbar\omega}\right)(g_1-g_R)K_1+(g_2-g_R)K_2+(g_3-g_R)K_3+\cdots\right]-K[(g_1-g_R)i_1+(g_2-g_R)i_2+(g_3-g_R)i_3+\cdots]\right\}^2\mu_N^2$$

where

$$K=K_1+K_2+K_3+\cdots.$$

In this formula the subscript 1 refers to the single quasiparticle in the system, and the subscripts 2, 3, ... refer to aligned quasiparticles or pairs of quasiparticles. In addition, i_n denotes the aligned angular momentum of the particle (or pairs of particles), and $\Delta e'$ represents the signature splitting. For the bands considered in the calculations the measured signature splitting is essentially zero. The values for the gyromagnetic factors g_R, g_1, g_2, g_3, the projection on the symmetry axis K_1, K_2, K_3, and the alignments i_1, i_2, and i_3 are listed in Table II. The value for g_R was determined experimentally using the method of nuclear magnetic resonance by two separate groups [18,19]. The g factors that are configuration dependent were taken from Refs. [20–22].

The $B(E2)$ value was calculated by

$$B(E2;I\rightarrow I-2)=\frac{5}{16\pi}Q_0^2\langle IK20|(I-2)K\rangle^2.$$

The value of Q_0, the intrinsic electric quadrupole moment, was determined by assuming that Q_0 is proportional to β_2, the quadrupole deformation parameter. Using the known value of Q_0 for ^{176}Hf, which is the core of ^{177}Ta, as tabulated by Raman *et al.* [23], and employing the calculated quadrupole deformation parameters of Nazarewicz *et al.* [24], Q_0 expectations can be calculated for the nuclear configurations in ^{177}Ta. These parameters are listed in Table II. The results for the theoretical calculations of $B(M1)/B(E2)$ are shown in Fig. 3 where very reasonable agreement can be seen as compared to the experimental values. The new strongly coupled structure is suggested to be a 3qp structure with a proposed configuration of $\pi[514]^{\frac{9}{2}-}\otimes\nu([633]^{\frac{7}{2}+},\ [521]^{\frac{1}{2}-})$. This assignment not only seems sensible from the observed bandhead spin and $B(M1)/B(E2)$ behavior but also from the measured aligned angular momentum; see Fig. 5 below. Other energetically possible configurations were investigated but were rejected since they did not fit the simultaneous requirements of fitting the experimental $B(M1)/B(E2)$ ratios, the bandhead spin value, and the aligned angular momentum conditions. For example, the $\pi[541]^{\frac{1}{2}-}\otimes\nu([624]^{\frac{9}{2}+},[514]^{\frac{7}{2}-})$ configuration was the only other candidate that satisfied the first two conditions but failed on the third because the alignment for the new strongly coupled band is less than that of the 1qp $[541]^{\frac{1}{2}-}$ band which would need the extra neutrons to add negative alignment, an unlikely result. In addition, the fact that the new strongly coupled band decays directly to the

TABLE II. Parameters for theoretical $B(M1)/B(E2)$ values for ^{177}Ta.

Band	Q_0	g_R	g_1	K_1	i_1	g_2	K_2	i_2	g_3	K_3	i_3
$\pi[402]^{\frac{5}{2}}$	6.1	0.35	1.46	2.5	0.0						
$\pi[404]^{\frac{7}{2}}$	6.6	0.35	0.80	3.5	0.0						
$\pi[514]^{\frac{9}{2}}$	6.6	0.35	1.26	4.5	0.32						
$\pi[402]^{\frac{5}{2}}\otimes\nu(i_{13/2})^2$	6.1	0.35	1.46	2.5	0.0	-0.21	0.0	8.9			
$\pi[404]^{\frac{7}{2}}\otimes\nu(i_{13/2})^2$	6.6	0.35	0.80	3.5	0.0	-0.21	0.0	8.9			
$\pi[514]^{\frac{9}{2}}\otimes\nu(i_{13/2})^2$	6.6	0.35	1.26	4.5	0.32	-0.21	0.0	8.9			
$\pi[514]^{\frac{9}{2}}\otimes\nu([633]^{\frac{7}{2}},[521]^{\frac{1}{2}})$	6.6	0.35	1.26	4.5	0.32	-0.21	3.5	2.9	1.0	0.5	0.31

$[514]\frac{9}{2}^-$ band and not the yrast $[541]\frac{1}{2}^-$ band suggests that the configuration most likely involves the $[514]\frac{9}{2}^-$ proton orbit.

IV. PROJECTED SHELL MODEL CALCULATIONS

The projected shell model (PSM), also called the angular momentum projection theory, has proven to be a powerful model to quantitatively account for many high-spin phenomena [25–29]. This is a shell model approach, but unlike the conventional shell model, the PSM begins with the deformed Nilsson [30] single-particle basis. Its advantage over the conventional shell model is that the important nuclear correlations, especially for a strongly deformed system, are easily taken into account in a manageable configuration space, thus making it possible to treat the heavy systems within the shell model framework. The results obtained from the PSM can be interpreted in simple physical terms. While our shell model basis violates the rotational symmetry, it can be restored by the standard angular momentum projection technique [31]. The pairing correlation is included by successive BCS calculations for the Nilsson states. Thus, the shell model truncation is carried out within the quasiparticle states with the vacuum $|\phi\rangle$. Recently, the model has been used to give a possible explanation for the problem of the anomalous crossing frequency in the odd-proton rare-earth nuclei [6].

The ansatz for the angular momentum projected wave function is given by

$$|IM\rangle = \sum_{\kappa} f_{\kappa}\hat{P}^{I}_{MK_{\kappa}}|\varphi_{\kappa}\rangle, \tag{1}$$

where κ labels the basis states. Acting on an intrinsic state $|\varphi_{\kappa}\rangle$, the operator $\hat{P}^{I}_{MK}$ [31] generates states of good angular momentum, thus restoring the necessary rotational symmetry violated in the deformed mean field. In the present work, we have assumed that the intrinsic states have axial symmetry. Thus, the basis states $|\varphi_{\kappa}\rangle$ must have K as a good quantum number. Since the nucleus in question has only a weak γ deformation, such a constraint will not prevent us from investigating the physics at hand. The basis states $|\varphi_{\kappa}\rangle$ are spanned by the set

$$\{\alpha^{\dagger}_{p_l}|\phi\rangle, \quad \alpha^{\dagger}_{n_i}\alpha^{\dagger}_{n_j}\alpha^{\dagger}_{p_l}|\phi\rangle\}$$
$$\{|\phi\rangle, \quad \alpha^{\dagger}_{n_i}\alpha^{\dagger}_{n_j}|\phi\rangle, \quad \alpha^{\dagger}_{p_k}\alpha^{\dagger}_{p_l}|\phi\rangle, \quad \alpha^{\dagger}_{n_i}\alpha^{\dagger}_{n_j}\alpha^{\dagger}_{p_k}\alpha^{\dagger}_{p_l}|\phi\rangle\}, \tag{2}$$

for odd-proton and even-even nuclei, respectively. The quasiparticle vacuum is $|\phi\rangle$ and α_m ($\alpha^{\dagger}_m$) is the quasiparticle annihilation (creation) operator for this vacuum; the index n_i (p_i) runs over selected neutron (proton) quasiparticle states and κ in Eq. (1) runs over the states in (2). The vacuum is obtained by diagonalizing a deformed Nilsson Hamiltonian [30] followed by a BCS calculation. In the calculation, we have used three major shells: i.e., $N = 4$, 5, and 6 ($N = 3$, 4, and 5) for neutrons (protons) as the configuration space. For the odd system, the BCS blocking effect associated with the last unpaired proton is taken into account by allowing all the odd number of protons to participate without blocking any individual level. Thus the vacuum in this case is an average over the two neighboring even-even nuclei. The size of the basis states, which includes the most important configurations, is determined by using energy cuts of 1.5, 2.5, 3, and 4 MeV for the 1qp, 2qp, 3qp, and 4qp states, respectively.

In this work we have used the Hamiltonian [27]

$$\hat{H}=\hat{H}_0-\tfrac{1}{2}\chi\sum_{\mu}\hat{Q}^{\dagger}_{\mu}\hat{Q}_{\mu}-G_M\hat{P}^{\dagger}\hat{P}-G_Q\sum_{\mu}\hat{P}^{\dagger}_{\mu}\hat{P}_{\mu}, \tag{3}$$

where $\hat{H}_0$ is the spherical single-particle shell model Hamiltonian. The second term is the quadrupole-quadrupole interaction and the last two terms are the monopole and quadrupole pairing interactions, respectively. The interaction strengths are determined as follows: The quadrupole interaction strength χ is adjusted so that the known quadrupole deformation ε_2 from the Hartree-Fock-Bogolyubov self-consistent procedure [32] is obtained. It turns out that for ^{177}Ta $\varepsilon_2 \simeq 0.25$. The monopole pairing strength G_M is adjusted to the known energy gap

$$G_M=\left[20.12\mp 13.13\frac{N-Z}{A}\right]A^{-1}, \tag{4}$$

where the minus (plus) sign is for neutrons (protons). The quadrupole pairing strength G_Q is assumed to be proportional to G_M and the proportional constant is fixed to be 0.18 in the present work.

The weights f_{κ} in Eq. (1) are determined by diagonalizing the Hamiltonian $\hat{H}$ in the basis given by Eq. (2). This will lead to the eigenvalue equation (for a given spin I)

$$\sum_{\kappa'}(H_{\kappa\kappa'}-EN_{\kappa\kappa'})f_{\kappa'}=0, \tag{5}$$

with the Hamiltonian and norm overlaps given by

$$H_{\kappa\kappa'}=\langle\varphi_{\kappa}|\hat{H}\hat{P}^{I}_{K_{\kappa}K'_{\kappa'}}|\varphi_{\kappa'}\rangle,$$
$$N_{\kappa\kappa'}=\langle\varphi_{\kappa}|\hat{P}^{I}_{K_{\kappa}K'_{\kappa'}}|\varphi_{\kappa'}\rangle. \tag{6}$$

Projection of good angular momentum onto each intrinsic state generates the rotational band associated with this intrinsic configuration $|\varphi_{\kappa}\rangle$. For example, $\hat{P}^{I}_{MK}\alpha^{\dagger}_{p_l}|\phi\rangle$ will produce a one-quasiproton band. The energies of each band are given by the diagonal elements of Eq. (6):

$$E_{\kappa}(I)=\frac{\langle\varphi_{\kappa}|\hat{H}\hat{P}^{I}_{KK}|\varphi_{\kappa}\rangle}{\langle\varphi_{\kappa}|\hat{P}^{I}_{KK}|\varphi_{\kappa}\rangle}=\frac{H_{\kappa\kappa}}{N_{\kappa\kappa}}. \tag{7}$$

The results obtained from diagonalizing the Hamiltonian of Eq. (3) will be compared with experiment below.

V. DISCUSSION

The excitation energy minus a rigid-rotor reference as a function of spin is plotted for ^{177}Ta in Fig. 4 for (a) the observed experimental bands and (b) the results of the PSM calculations. An aligned angular momentum plot for the experimental bands observed in ^{177}Ta is shown in Fig. 5(a).

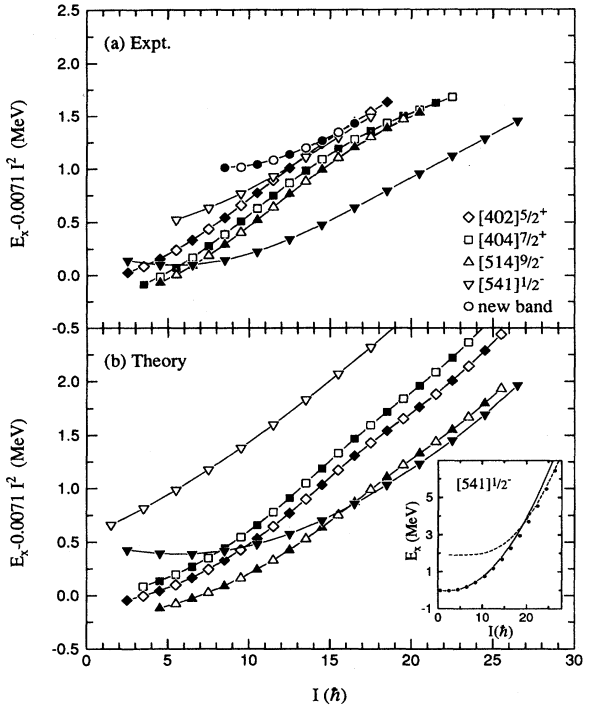

FIG. 4. Excitation energy minus a rigid-rotor reference as a function of spin for (a) the observed experimental bands and (b) the predictions of the PSM calculations. The inset in panel (b) shows the crossing of the 1qp and 3qp bands for the $[541]\frac{1}{2}^-$ favored orbital as predicted by the PSM. The open and solid symbols differentiate between signatures of the same Nilsson configuration.

The reference Harris parameters $\mathcal{J}_0 = 35\hbar^2$ MeV^{-1} and $\mathcal{J}_1 = 15\hbar^4$ MeV^{-3} were obtained from a parameterization of the ground-state band of the neighboring even-even nucleus ^{176}Hf following the prescription of Bengtsson and Frauendorf [33,34]. Figure 5(b) shows the results of the same procedure applied to the results of the PSM calculations. Figure 5 also contains the yrast band of ^{176}Hf from experiment and theory which is included for comparison purposes.

In Fig. 4 the general excitation behavior as a function of spin of the lowest-lying proton orbitals $[541]\frac{1}{2}^-$, $[404]\frac{7}{2}^+$, $[402]\frac{5}{2}^+$, and $[514]\frac{9}{2}^-$ is well reproduced in the calculations although the $[514]\frac{9}{2}^-$ band is predicted a little too low in energy and the ordering of the two positive-parity orbitals is reversed. The signature splitting of the $[541]\frac{1}{2}^-$ band is slightly overestimated by about 300 keV at $I = 10\hbar$. We understand that this deviation comes from the basis truncation. The unfavored levels of this band lie close to the truncated boundary, and, therefore, there are not enough neighboring bands to push them down. Comparing between experiment and the theoretical predictions of the PSM at low rotational frequencies in more detail, the alignment plots shown in Fig. 5 indicate that the $[514]\frac{9}{2}^-$ band is predicted to have slightly too high an alignment compared with the $[404]\frac{7}{2}^+$ and $[402]\frac{5}{2}^+$ bands. This result is consistent with the slightly too low excitation energy of the $[514]\frac{9}{2}^-$ band in the calculations. A similar comparison for the lower than observed alignment for the unfavored $[541]\frac{1}{2}^-$ band is also consistent with the higher than observed signature splitting predicted for the $[541]\frac{1}{2}^-$ orbital. Considering that all bands in the discussion are obtained by one diagonalization without individual parameter adjustment, the results are satisfactory.

A. Identical bands at low spins

The occurrence of bands with "identical" moments of inertia in neighboring normal deformed nuclei is currently attracting a great deal of attention; see [35] for a comprehensive discussion and complete list of references. Some of the best cases occur in odd-Z nuclei around $A = 175$ and include ^{177}Ta [2,3]. In ^{177}Ta, both signatures of the $[402]\frac{5}{2}^+$ structure at low spin have "identical" moments of inertia to the ground-state band in the neighboring even-even nucleus

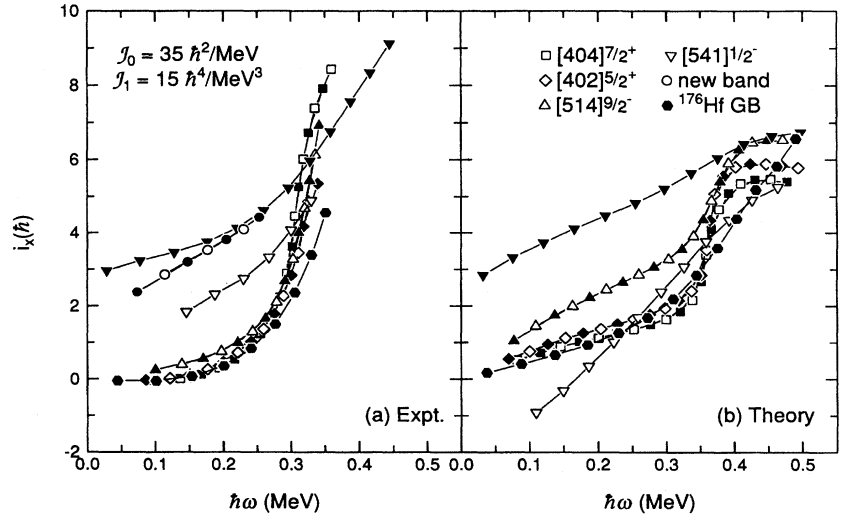

FIG. 5. Aligned angular momentum as a function of rotational frequency for (a) the observed bands in ^{177}Ta and the ground-state band in ^{176}Hf and (b) the results from the PSM calculations. The open and solid symbols differentiate between signatures of the same Nilsson configuration.

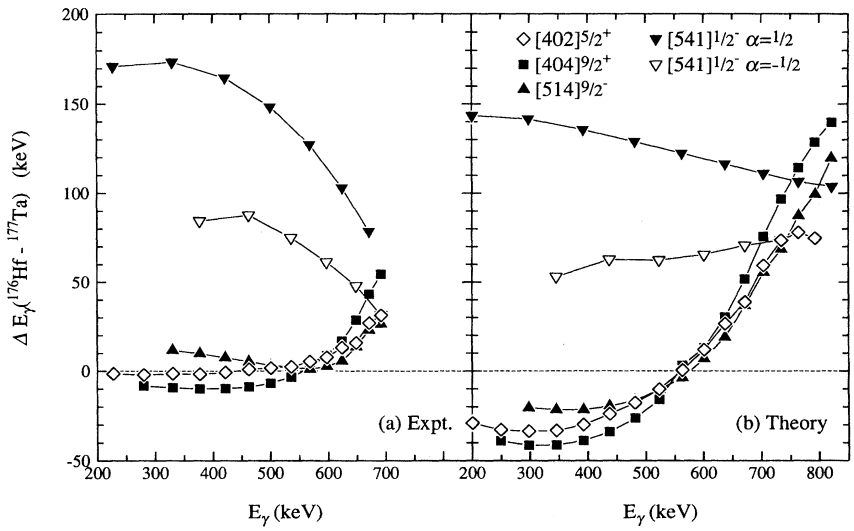

FIG. 6. The difference in transition energies between the ^{176}Hf ground-state band (averaged to achieve the appropriate spin values) and the various configurations in ^{177}Ta as a function of spin for (a) the experimentally observed quantities and (b) the PSM calculated values.

^{176}Hf. This feature is illustrated in Fig. 6(a) where the difference in transition energies between the ground-state band in ^{176}Hf (with appropriate spin averaging) and bands in ^{177}Ta is shown. The divergence away from the ^{176}Hf reference (zero line) of the $[402]\frac{5}{2}^+$ band at high spin observed in the present work was taken as evidence for a slightly lower crossing frequency at the first $i_{13/2}$ neutron crossing (see below) for the $[402]\frac{5}{2}^+$ band. This result [4] gave an experimental indication that the deformation of the $[402]\frac{5}{2}^+$ band was less than that of the ground-state band in ^{176}Hf which was consistent with the pairing-deformation cancellation proposal for the occurrence of "identical bands" [1,2]. The experimental $[404]\frac{7}{2}^+$ and $[514]\frac{9}{2}^-$ bands also track the reference reasonably closely in a similar manner to the $[402]\frac{5}{2}^+$ band and, as expected, the $[541]\frac{1}{2}^-$ bands show quite different behavior.

In Fig. 6(b) the equivalant theoretical PSM results for the bands in ^{177}Ta referenced to the theoretically calculated ground-state band in ^{176}Hf are shown. While the "identical" nature of the $[402]\frac{5}{2}^+$ band in ^{177}Ta and the ground-state band in ^{176}Hf is not perfectly reproduced, the general trends certainly are. This is true both for the correct ordering of the $[514]\frac{9}{2}^-$, $[402]\frac{5}{2}^+$, and $[404]\frac{7}{2}^+$ bands as well as the splitting of the $[541]\frac{1}{2}^-$ sequences.

B. The first $i_{13/2}$ neutron crossing and the $h_{9/2}$ anomaly

In each rotational sequence based on a single-quasiproton orbital, the first $i_{13/2}$ neutron alignment is expected to occur at about the same rotational frequency ($\hbar\omega_c \sim$ 0.3 MeV). This simple expectation is confirmed experimentally except for bands based on the $[541]\frac{1}{2}^-$ orbital. In this latter case, the alignment is systematically delayed in rotational frequency compared with the other bands. This is illustrated in Fig. 7 where the experimentally measured band crossing frequencies ($\hbar\omega_c$) for a wide range of Hf and Ta isotopes are plotted as a function of neutron number.

The explanation of this delayed alignment has been a long-standing problem in odd-proton nuclei. The occupation of the $[541]\frac{1}{2}^-$ orbital is expected to drive the nucleus to a larger deformation. Although this increased deformation will cause an increase in $\hbar\omega_c$, it cannot explain the full extent of the observed delay. PSM calculations have recently been able to reproduce in a consistent manner the delayed backbending observed in $h_{9/2}$ bands in a long chain of Ta isotopes from $A=167$ to 175 [6]. In the present work the same framework is used to perform calculations for ^{177}Ta where the crossing frequency might be expected to be largest; see Fig. 7.

To discuss the first $i_{13/2}$ neutron crossing it is informative to use the aligned angular momentum plots shown in Fig. 5. In Fig. 5(a) the sharp rise in i_x around $\hbar\omega = 0.3$ MeV in the

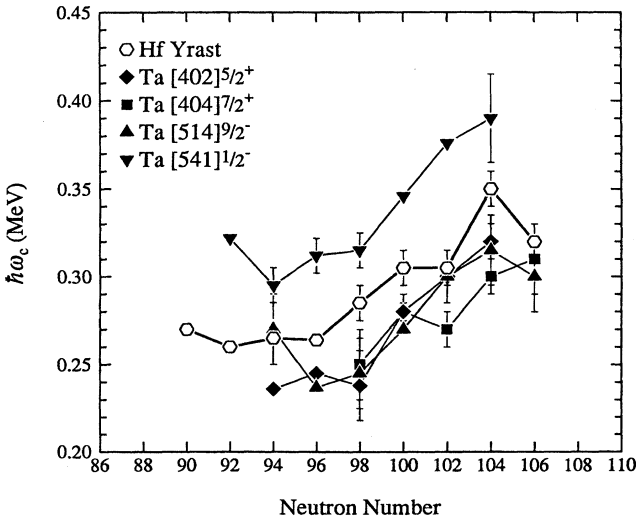

FIG. 7. Plot of observed crossing frequency for the first $\nu i_{13/2}$ alignment as a function of neutron number for even-even Hf isotopes and the $[541]\frac{1}{2}^-$, $[404]\frac{7}{2}^+$, $[402]\frac{5}{2}^+$, and $[514]\frac{9}{2}^-$ configurations in Ta isotopes.

$[402]\frac{5}{2}^+$, $[514]\frac{9}{2}^-$, and $[404]\frac{7}{2}^+$ bands is due to the alignment of the first pair of $i_{13/2}$ neutrons. An alignment gain of $\Delta i_x > 8\hbar$ [extrapolating slightly, we estimate a value of $\Delta i_x \sim (9-10)\hbar$] observed in the $[404]\frac{7}{2}^+$ band is consistent with this interpretation. The observation that these bands all exhibit very similar behavior fits in well with the expectations of these bands having comparable deformations [24]. The ground-state band in ^{176}Hf also backbends at a slightly higher rotational frequency, again in line with our expectations.

The $[541]\frac{1}{2}^-$ band clearly has very different alignment behavior [see Fig. 5(a)] to most of the other bands in ^{177}Ta with the favored signature passing smoothly through, for example, the $[404]\frac{7}{2}^+$ band at $\hbar\omega = 0.3$ MeV and extending up to a maximum observed rotational frequency of $\hbar\omega = 0.45$ MeV. In ^{175}Ta the favored $h_{9/2}$ band also exhibits quite smooth behavior until a sharp backbend is observed at $\hbar\omega = 0.4$ MeV [36,37]. This latter crossing was then interpreted as the $i_{13/2}$ neutron backbend. The large crossing frequency value for ^{175}Ta can be seen in Fig. 7. The question then arises with regard to Fig. 7, that if because no sharp backbend in the $[541]\frac{1}{2}^-$ band in ^{177}Ta is observed up to $\hbar\omega = 0.45$ MeV, should one place a lower limit at this particular rotational frequency on this graph or not? This would certainly continue the trend for the Ta isotopes to higher critical rotational frequency values but one must worry about the physical cause for such an enormously delayed backbending.

Instead we propose a different interpretation for what is taking place in the $[541]\frac{1}{2}^-$ band in ^{177}Ta. In Fig. 5 the $[541]\frac{1}{2}^-$ band has an initial alignment $i_x = 3\hbar$. With increasing rotational frequency, in particular above $\hbar\omega \sim 0.25$ MeV, the $[541]\frac{1}{2}^-$ band gains in alignment compared to the reference. This behavior also occurs for the $[402]\frac{5}{2}^+$,$[404]\frac{7}{2}^+$, and $[514]\frac{9}{2}^-$ bands and is due to the first $\nu i_{13/2}$ band crossing as discussed above. We suggest that this band crossing is also taking place in the $[541]\frac{1}{2}^-$ band, but, in contrast to the other bands, it involves a much stronger interaction strength. The extraction of a specific crossing frequency is therefore slightly harder to determine. However, if we assume that an alignment gain $\Delta i_x \sim 9\hbar$ also takes place in the $[541]\frac{1}{2}^-$ band due to the neutron alignment, we may estimate a crossing frequency of $\hbar\omega_c \sim 0.39$ MeV from the point ($i_x \simeq 7.5\hbar$) at which half of the expected alignment gain is reached. This estimate for ^{177}Ta is shown in Fig. 7 and is consistent with the systematic trends. A band observed to high rotational frequency in ^{176}Ta [38] may also be used to support our interpretation. The large alignment of this band taken together with its strong population led us to suggest that it has the configuration $\pi h_{9/2} \otimes \nu i_{13/2}$. This assignment is then consistent with the observation that the first $i_{13/2}$ band crossing is blocked and the experimental fact that relative to this ^{176}Ta band the $[541]\frac{1}{2}^-$ band in ^{177}Ta gains gradually but noticeably in alignment at frequency values above 0.3 MeV.

The theoretical PSM calculations also support this interpretation where the inset of Fig. 4(a) shows the diabatic trajectories for the $[541]\frac{1}{2}^-$ 1qp and aligned 3qp bands. The bands cross with a sizable interaction strength ($V_{\rm int} \approx$ 1 MeV), at a spin of about $I = \frac{37}{2}$, which corresponds to a rotational frequency of about $\hbar\omega \simeq 0.36$ MeV. The theoretical alignment plot in Fig. 5(b), while not reproducing the full i_x gain, does show gradual upsloping behavior near this rotational frequency. The predicted PSM change in behavior of the interaction strength at the first $i_{13/2}$ band crossing for the $[541]\frac{1}{2}^-$ band in a range of Ta isotopes is shown in Fig. 8. The general oscillatory nature of the interaction strength as a function of neutron number is well known [33,39,40], but it is interesting that an especially large jump in $V_{\rm int}$ is predicted between ^{175}Ta and ^{177}Ta. In fact the calculations predict extremely well the complete trend for $^{169-177}$Ta isotopes as

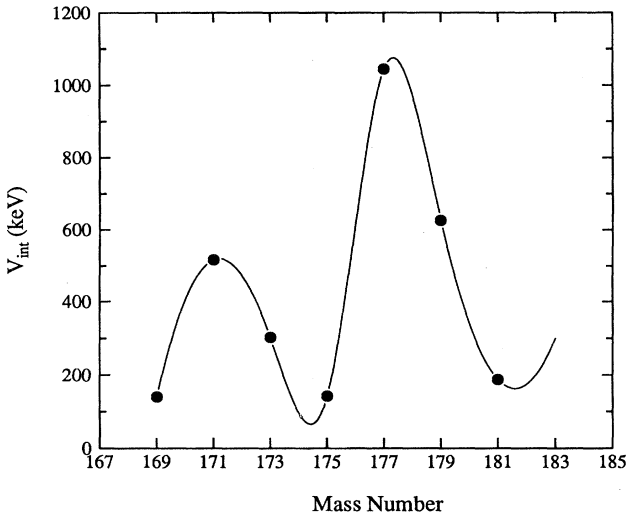

FIG. 8. The PSM calculated interaction strength $V_{\rm int}$ for the first $\nu i_{13/2}$ crossing in the $h_{9/2}[541]\frac{1}{2}^-$ sequence as a function of neutron number for the odd-A Ta isotopes.

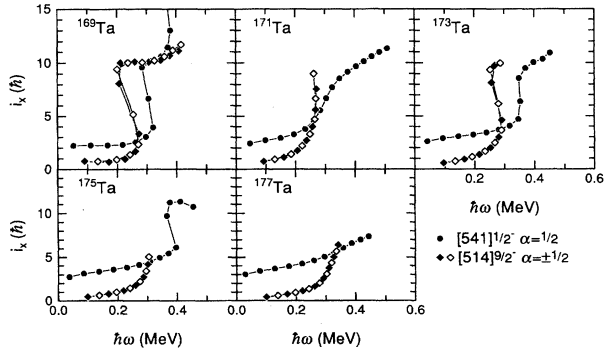

FIG. 9. Aligned angular momentum as a function of rotational frequency for the $h_{9/2}[541]\frac{1}{2}^-$ bands in the even-neutron Ta isotopes from $A = 169$ to $A = 177$. The Harris parameters used in the plots are $\mathcal{J}_0 = 33\hbar^2$ MeV^{-1} and $\mathcal{J}_1 = 45\hbar^4$ MeV^{-3}. For each nucleus the $[514]\frac{9}{2}^-$ band has been included for comparison. The data sources are as follows: ^{169}Ta [20], ^{171}Ta [42], ^{173}Ta [43], ^{175}Ta [36,38].

illustrated in Fig. 9, where the size of the interaction strength can be estimated from the "sharpness" of the large alignment gain near $\hbar\omega \sim$ 0.3–0.35 MeV. In addition, the calculations correctly predict a local maximum (see Fig. 8) for the interaction strength for ^{171}Ta, where in Fig. 9 there is a more gradual alignment gain for this isotope in comparison with its odd-isotope neighbors ^{169}Ta and ^{173}Ta. A more complete discussion of the changing interaction strength with neutron number using the PSM will be the topic of a separate publication [41].

VI. CONCLUSIONS

Rotational band structures in ^{177}Ta have been studied at high spins. Considerable extensions have been made to the previously known level scheme and a new proposed 3qp structure has been found. $B(M1)/B(E2)$ ratios have been extracted for the strongly coupled bands, and they are shown to agree with our configuration assignments. The anomalous crossing frequency observed in the $[541]\frac{1}{2}^-$ proton $h_{9/2}$ band at the first $i_{13/2}$ neutron alignment has been discussed, and for this crossing in ^{177}Ta a large interaction strength has been proposed. Detailed comparisons have been made with projected shell model calculations, in particular regarding the characteristics of the first $i_{13/2}$ neutron crossing and the occurrence of "identical bands."

ACKNOWLEDGMENTS

Special thanks to D. C. Radford, H. Q. Jin, and W. T. Milner for their wonderful software support. Thanks also to F. K. McGowan, N. R. Johnson, and R. Darlington for their marvelous help with the targets and to the accelerator staff at FSU. This work was supported by the National Science Foundation and the State of Florida and by the UK Science and Engineering Research Council. M.A.R. and J.S. acknowledge the receipt of a NATO Collaborative Research Grant.

[1] J.-Y. Zhang, R.F. Casten, W.-T. Chou, D.S. Brenner, N.V. Zamfir, and P. von Brentano, Phys. Rev. Lett. **69**, 1160 (1992).
[2] J.-Y. Zhang and L.L. Riedinger, Phys. Rev. Lett. **69**, 3448 (1992).
[3] C. Baktash, J.D. Garrett, D.F. Winchell, and A. Smith, Phys. Rev. Lett. **69**, 1500 (1992).
[4] M.A. Riley, D.E. Archer, J. Simpson, T.B. Brown, J. Döring, J.W. Holcomb, G.D. Johns, T.D. Johnson, T. Petters, J. Pfohl, S.L. Tabor, O.N. Tekyi-Mensah, P.C. Womble, and V.A. Wood, Z. Phys. A **346**, 319 (1993).
[5] L.L. Riedinger *et al.*, Prog. Part. Nucl. Phys. **28**, 75 (1992).
[6] Y. Sun, S. Wen, and D.H. Feng, Phys. Rev. Lett. **72**, 3483 (1994).
[7] C.S. Wu, Phys. Rev. C **51**, 1819 (1995).
[8] M. Dasgupta, P.M. Walker, G.D. Dracoulis, A.P. Byrne, P.H. Regan, T. Kibédi, G.J. Lane, and K.C. Yeung, Phys. Lett. B **328**, 16 (1994).
[9] M. Dasgupta, A.P. Byrne, G.D. Dracoulis, T. Kibédi, F.G. Kondev, G.J. Lane, P.H. Regan, P.M. Walker, and K.C. Yeung, Annual Report, Department of Nuclear Physics, Australian National University, 1994, p. 20.
[10] J.F. Sharpey-Schafer and J. Simpson, Prog. Part. Nucl. Phys. 21, 293 (1988).
[11] S.L. Tabor, M.A. Riley, J. Döring, P.D. Cottle, R. Books, T. Glasmacher, J.W. Holcomb, J. Hutchins, G.D. Johns, T.D. Johnson, T. Petters, O. Tekyi-Mensah, P.C. Womble, L. Wright, and J.X. Saladin, Nucl. Instrum. Methods B **79**, 821 (1993).
[12] D.C. Radford, in Proceedings of International Conference on Nuclear Structure at High Angular Momentum and Workshop on Large Gamma-Ray Detector Arrays, Ottawa and Chalk River, 1992 (unpublished), Vol. 2, p. 403 and Nucl. Instrum. Methods (submitted).
[13] D. Barnéoud, C. Foin, A. Baudry, A. Gizon, and J. Valentin, Nucl. Phys. **A154**, 653 (1970).
[14] B. Skanberg, S.A. Hjorth, and H. Ryde, Nucl. Phys. **A154**, 641 (1970).
[15] K.D. Schilling, W. Andrejtscheff, F. Dubbers, and P. Manfrass, Nucl. Phys. **A208**, 417 (1973).
[16] V.P. Janzen, Z.-M. Liu, M.P. Carpenter, L.H. Courtney, H.-Q. Jin, A.J. Larabee, L.L. Riedinger, J.K. Johansson, D.G. Popescu, J.C. Waddington, S. Monaro, S. Pilotte, and F. Dönau, Phys. Rev. C **45**, 613 (1992).
[17] F. Dönau, Nucl. Phys. **A471**, 469 (1987).
[18] E. Hagn and E. Zech, Nucl. Phys. **A369**, 205 (1981).
[19] S. Ohya, K. Nishimura, A. Furusawa, and N. Mutsuro, J. Phys. Soc. Jpn. **53**, 2479 (1984).
[20] S.G. Li, S. Wen, G.J. Yuan, G.S. Li, P.F. Hua, L.K. Zhang, Z.K. Yu, P.S. Yu, P.K. Weng, C.X. Yang, R. Chapman, D. Clarke, F. Khazaie, J.C. Lisle, J.N. Mo, J.D. Garrett, G.B. Hagemann, B. Herskind, and H. Ryde, Nucl. Phys. **A555**, 435 (1993).
[21] C.-H. Yu, G.B. Hagemann, J.M. Espino, K. Furuno, J.D. Garrett, R. Chapman, D. Clarke, F. Khazaie, J.C. Lisle, J.N. Mo, M. Bergström, L. Carlén, P. Ekström, J. Lyttkens, and H. Ryde, Nucl. Phys. **A511**, 157 (1990).
[22] P. Raghavan, At. Data Nucl. Data Tables **42**, 189 (1989).
[23] S. Raman, C.H. Malarkey, W.T. Milner, C.W. Nestor, Jr., and P.H. Stelson, At. Data Nucl. Data Tables **36**, 1 (1987).
[24] W. Nazarewicz, M.A. Riley, and J.D. Garrett, Nucl. Phys. **A512**, 61 (1990).
[25] K. Hara and S. Iwasaki, Nucl. Phys. **A332**, 61 (1979).
[26] K. Hara and S. Iwasaki, Nucl. Phys. **A348**, 200 (1980).
[27] K. Hara and Y. Sun, Nucl. Phys. **A529**, 445 (1991).
[28] K. Hara and Y. Sun, Nucl. Phys. **A531**, 221 (1991).
[29] K. Hara and Y. Sun, Nucl. Phys. **A537**, 77 (1992).
[30] C.G. Andersson, G. Hellström, G. Leander, I. Ragnarsson, S. Åberg, J. Krumlinde, S.G. Nilsson, and Z. Szymański, Nucl. Phys. **A309**, 141 (1978).
[31] P. Ring and P. Schuck, *The Nuclear Many Body Problem* (Springer-Verlag, Berlin, 1980).
[32] I.L. Lamm, Nucl. Phys. **A125**, 504 (1969).
[33] R. Bengtsson and S. Frauendorf, Nucl. Phys. **A327**, 139 (1979).
[34] R. Bengtsson, S. Frauendorf, and F.-R. May, At. Data Nucl. Data Tables **35**, 15 (1986).

[35] C. Baktash, B. Haas, and W. Nazarewicz, Annu. Rev. Nucl. Part. Sci. (to be published).
[36] W. Shuxian, Z. Hua, L. Shenggang, L. Guangsheng, Y. Guanjun, H. Pengfei, W. Peikun, Z. Lankuan, Y. Panshui, J. Fangxian, Y. Chunxiang, S. Huibin, L. Yabo, and L. Yunzuo, Z. Phys. A **339**, 417 (1991).
[37] S. Wen, H. Zheng, S.G. Li, G.S. Li, G.J. Yuan, P.F. Hua, P.K. Weng, L.K. Zhang, P.S. Yu, C.X. Yang, H.B. Sun, Y.B. Lui, Y.Z. Lu, Y. Sun, and D. Feng (unpublished).
[38] D.E. Archer *et al.* (unpublished).
[39] R. Bengtsson, I. Hamamoto, and B. Mottelson, Phys. Lett. **73B**, 259 (1978).
[40] Y. Sun, P. Ring, and R.S. Nikam, Z. Phys. A **339**, 51 (1991).
[41] Yang Sun *et al.* (unpublished).
[42] J.C. Bacelar, R. Chapman, J.R. Leslie, J.C. Lisle, J.N. Mo, E. Paul, A. Simcock, J.C. Willmott, J.D. Garrett, G.B. Hagemann, B. Herskind, A. Holm, and P.M. Walker, Nucl. Phys. **A442**, 547 (1985).
[43] H. Carlsson, L.P. Ekström, A. Nordlund, H. Ryde, R.A. Bark, G.B. Hagemann, S.J. Freeman, H.J. Jensen, H. Schnack-Petersen, F. Ingebretsen, P.O. Tjøm, T. Lönnroth, and M.P. Piiparinen (unpublished).